GENERAL SYMPOSIA | FIBERS AND FILMS

Polyketone-Polypropylene Core-Shell Fibers for Concrete Reinforcement

Jonas Herz, Sophia Hefenbrock, Katharina Lorenz, Dirk Muscat and Nicole Strübbe

DOI: https://doi.org/10.51573/Andes.PPS39.GS.FF.1

December 2024

View Online

Export Citation

Polyketone-Polypropylene Core-Shell Fibers for Concrete Reinforcement

Jonas Herz, Sophia Hefenbrock, Katharina Lorenz, Dirk Muscat and Nicole Strübbe[1]

Abstract: Corrosion of commonly used steel reinforcements weakens the structural strength of concrete. To address this issue, research was conducted on concrete reinforcements in the form of polymer fibers. These polymer fibers need concrete bonding ability and good mechanical properties. This study investigates core-shell fibers produced from polyketone and polypropylene mixed with a compatibilizer. The core-shell fibers were produced by coextrusion and drawing. The fibers were analyzed by tensile tests, a single fiber pull-out test, contact angle measurements, scanning electron microscopy, and thermogravimetric analysis.

Keywords: Concrete Reinforcement, Core-Shell Fiber, Polyketone, Polypropylene

1 The authors Jonas Herz (jonas.herz@th-rosenheim.de), Sophia Hefenbrock, Katharina Lorenz, Dirk Muscat and Nicole Strübbe are affiliated with the Faculty of Engineering at the Rosenheim Technical University of Applied Sciences in Germany.

DOI: https://doi.org/10.51573/Andes.PPS39.GS.FF.1

Introduction

Concrete is currently the principal material used in the building industry [1]. However, because of the corrosion of steel reinforcements, the concrete industry is searching for alternative reinforcement possibilities. Different solutions, like stainless steel [2] as well as carbon fiber reinforcements [3] and polymer fibers [4], have been investigated. To be considered an alternative reinforcement, a polymer fiber needs to simultaneously provide high mechanical properties and good bonding ability to the concrete matrix [5]. However, other fiber properties should also be considered. In case of fire, decomposition of polymer fibers creates a porous system. This porous system allows vapor to clear out of the concrete with decreased spalling [6]. Accordingly, tests concerning the thermal stability are also performed. Previous research indicated good bonding abilities through the addition of calcium carbonate and wood particles in the shell of polypropylene (PP) core-shell fibers [7]. Further, polyketone (PK) showed high mechanical properties [8]. Nevertheless, the processing temperature of PK is too high for the addition of wood particles. As a first step in this direction, this research investigates core-shell fibers that combining PK in the core and PP in the shell, in relation to their mechanical properties, concrete bonding ability, and thermal stability. A subsequent addition of filler particles to the shell material could be considered for future research.

Experiments

Materials

A combination of three materials was used in this research. An aliphatic polyketone with a density of 1.19 g/cm³ and a melt volume rate of 21 g/10 min at 240°C and 5 kg [9] was used as core material. In the shell, polypropylene with a density of 0.905 g/cm³ and a melt flow rate (MFR) of 1 g/10 min at 230°C and 2.16 kg [10] was used as base material. A maleic anhydride grafted polypropylene (MAH) with a density of 0.91 g/cm³ and a melt flow rate of 9.1 g/10 min at 230°C and 2.16 kg [11] worked as a compatibilizer to the PP in the shell.

Processing

Compounding

Three different shell-material combinations were compounded using a Coperion ZSK 26 MC^{18} twin screw extruder with a screw diameter of 26 mm and a l/d-ratio of 48. The MAH was added to the PP by 25, 50, and 75 wt.-%. The compounding parameters are shown in Table 1.

DOI: https://doi.org/10.51573/Andes.PPS39.GS.FF.1

Table 1. Compounding parameters for shell-material production.

Shell Material	Screw Speed	Mass Temperature	Pressure	Throughput
	[rpm]	[°C]	[bar]	[kg/h]
PP75-MAH25	250	227	21	12
PP50-MAH50	250	227	25	12
PP25-MAH75	250	225	18	12

Fiber Production

The core-shell fibers were processed by a two-step process. First, a strand was produced using coextrusion. The same Coperion ZSK 26 MC[18] twin screw extruder used for compounding the shell materials was connected to a HAAKE polydrive single screw extruder with a screw diameter of 19 mm and a l/d-ratio of 25 via a coextrusion die. The core material (C) was processed by the twin screw extruder (Extruder 1) and the shell material (S) by the single screw extruder (Extruder 2). After extrusion, the strand was cooled in a water bath and taken-up by a godet. The coextrusion parameters are shown in Table 2. Second, the strand was drawn to a fiber using a Collin Teach Line MDO stretching unit. The strand was placed in front of the stretching unit. The speed of the first godet before the furnace was set at 1 m/min. Fiber drawing was induced by temperature and tension applied by a higher speed of the second godet after the furnace. The roll-temperature of both godets was set at 80°C and the furnace was heated up to 188°C. All fibers were drawn until fiber failure occurred. A draw ratio (DR) was calculated by the ratio between the speeds of the two godets.

Table 2. Coextrusion parameters for strand production.

Fiber	Extruder 1				Extruder 2			Strand Handling	
	Screw Speed	Mass Temperature	Pressure	Throughput	Screw Speed	Mass Temperature	Pressure	Water-bath Temperature	Take-up Speed
	[rpm]	[°C]	[bar]	[kg/h]	[rpm]	[°C]	[bar]	[°C]	[m/min]
C-PK-S-PP100	120	237	98	1.5	17	210	125	20	12
C-PK-S-PP75-MAH25	120	237	112	1.5	17	209	72	14	12
C-PK-S-PP50-MAH50	120	237	112	1.5	17	209	59	14	12
C-PK-S-PP25-MAH75	120	237	110	1.5	14	208	45	14	12

DOI: https://doi.org/10.51573/Andes.PPS39.GS.FF.1

Fiber Analysis

The mechanical properties of the fibers were examined by tensile tests using a Zwick universal testing machine (Z100) equipped with a 10 kN load cell and 90° deflection grips. The sample length was 250 mm. The test speed was set at 1 mm/min during determination of Young's modulus and increased to 10 mm/min until fiber break. Five samples were tested per fiber material.

Single fiber pull-out tests (SFPT) were used to investigate the bonding between fiber and concrete. For specimen preparation, single fibers were fixed with 15 mm embedment length in molds with a size of 60 x 60 x 30 mm³. The molds were filled with the concrete mixture presented in Table 3. The concrete mixture was manufactured using a Kitchen Aid ProLine Series 6 equipped with a flat beater. First, the concrete was cured for 24vh in a climate-regulated chamber at a humidity of 67% and a temperature of 20°C. Then, the specimens were demolded and stored for another 13 days in the same environment as the first curing step. Finally, six specimens per fiber material were tested at a specimen curing time of 14 days using a Zwick universal testing machine (Zwick 1474) equipped with a 500 N load cell. The pull-out speed was 2 mm/min. The test ended after complete fiber pull-out. As the fiber was clamped directly on top of the specimen surface, the free fiber length can be ignored.

Table 3. Concrete mixture.

Material		Sand	Portland Cement (CEM I)	Limestone	Water	Superplasticizer 1	Superplasticizer 2
Amount	[g]	1350	450	75	220	6.2	3.0

For every fiber, the interfacial shear strength (IFSS) τ_{IFSS} was calculated from the pull-out curves by:

$$\tau_{IFSS} = \frac{F_{max}}{\pi\, d_f l_e} \quad (1)$$

where F_{max} represents the maximum extraction force, d_f the equivalent fiber diameter, and l_e the embedment length.

Surface energies and polarities of the core-shell fibers were examined at their maximum DR using contact angle measurements by a KRÜSS EasyDrop FM40. The test liquids used were water and diiodomethane. The fiber surfaces were cleaned, and eight small droplets of each liquid were set on the surface to measure the contact angle. The calculation of the surface energy was done using the Krüss ADVANCE software accordingly to the method of Owen, Wendt, Rabel, and Kaelble. This method allows splitting of the surface energy into a dispersive and a polar part [12].

DOI: https://doi.org/10.51573/Andes.PPS39.GS.FF.1

Optical analysis of the different fiber surfaces prior and after SEPT was performed on the scanning electron microscope MIRA3 from Tescan using the secondary electron detector. The samples were gold sputtered and inspected at different magnifications using an accelerating voltage of 10kV.

The fiber decomposition was tested via thermogravimetric analysis (TGA) using a TA Instruments TGA 5500. The different fibers were analyzed under nitrogen atmosphere at temperatures between ≈30°C and 650°C at a heat rate of 20 K/min. The mass loss was recorded as a function of temperature.

Results and Discussion

Fiber Production

The furnace temperature for all fibers was above the melting temperature of PP to draw the PK core. Similarly to the argument in previous research, this could be caused by a high melt stiffness of the PP [8]. The maximum DR and the equivalent fiber diameters are shown in Table 4.

Table 4. Attained draw ratios and fiber diameters.

Shell Material		C-PK-S-PP100	C-PK-S-PP75-MAH25	C-PK-S-PP50-MAH50	C-PK-S-PP25-MAH75
Maximum Draw Ratio	[1]	10	9	8	9
Equivalent Fiber Diameter	[mm]	0.54 ± 0.2	0.57 ± 0.1	0.62 ± 0.1	0.58 ± 0.1

Tensile Tests

The results from tensile tests are presented in Figure 1. The highest Young's modulus is reached by C-PK-S-PP100, and C-PK-SPP50-MAH50 shows the lowest value. In case of the materials containing MAH, the Young's modulus seems to follow the DR. C-PK-SPP75-MAH25 shows the highest tensile strength, while higher amounts of MAH decrease the tensile strength. This could be a result of the shorter polymer chains of the MAH, which are indicated by the higher MFR compared to the PP.

DOI: https://doi.org/10.51573/Andes.PPS39.GS.FF.1

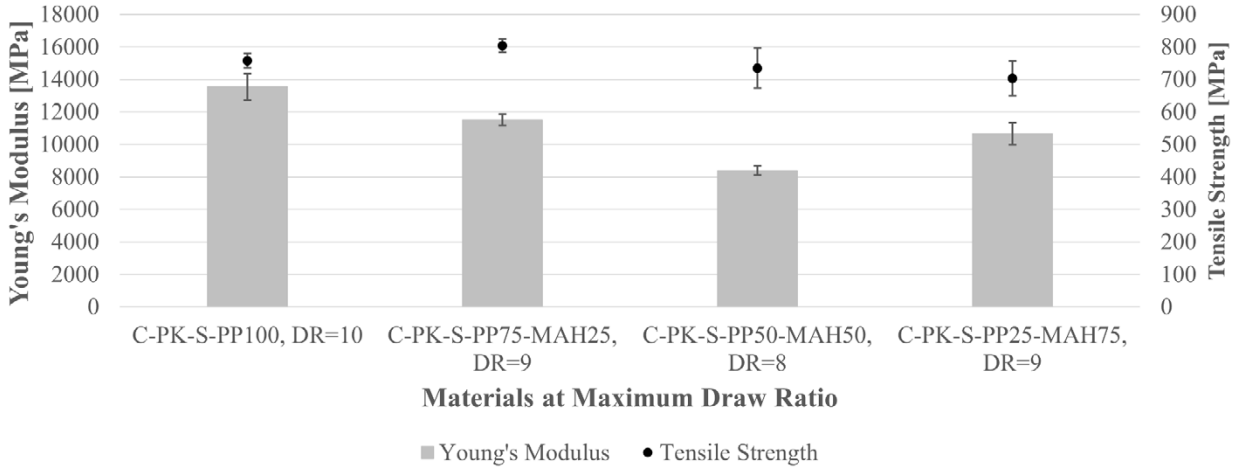

Figure 1. Results from tensile tests.

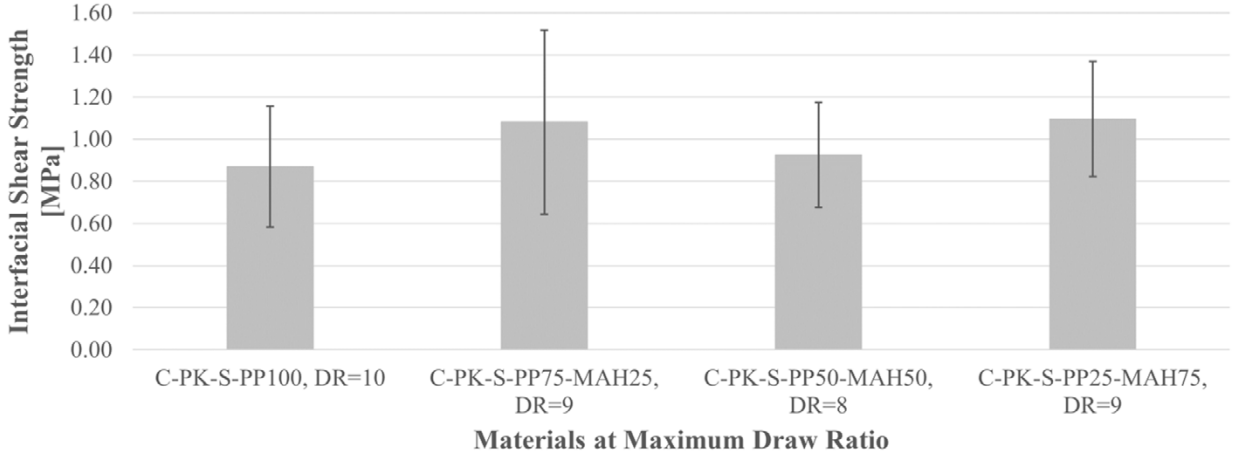

Figure 2. Results from single fiber pull-out tests.

Single Fiber Pull-out Tests

The results from SFPT in Figure 2 demonstrate an increased IFSS for the materials containing MAH. Further, a comparison with Figure 1 indicates a correlation of IFSS and Young's modulus for the MAH containing fibers. As the Young's modulus is influenced by the DR, the DR could also be considered an influencing factor on the IFSS. Nevertheless, the influence of MAH and the Young's modulus respectively DR on the IFSS seems to be rather small.

DOI: https://doi.org/10.51573/Andes.PPS39.GS.FF.1

Contact Angle Measurements

An increase in surface energy for the fibers containing MAH is clearly visible in Figure 3. A slightly increased polarity is also shown. Furthermore, surface energy correlates with the IFSS presented in Figure 2, which allows the assumption that the higher surface energy causes a better wetting of the fiber surface by the concrete.

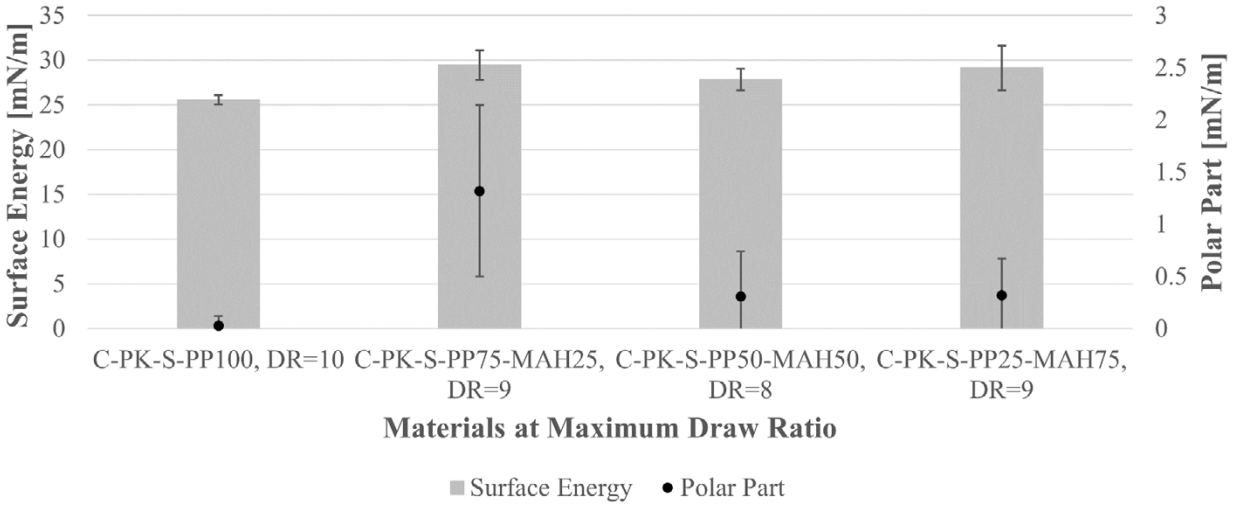

Figure 3. Results from contact angle measurements.

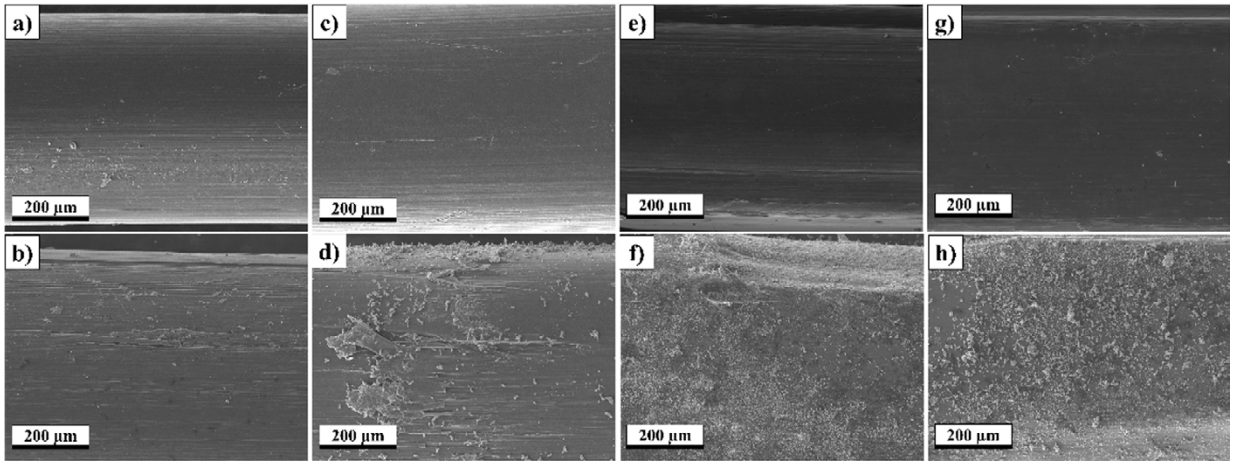

Figure 4. Scanning electron microscopy pictures, C-PK-S-PP100, DR=10 before a) and after b) pull-out, C-PK-S-PP75-MAH25, DR=9 before c) and after d) pull-out, C-PK-S-PP50-MAH50, DR=8 before e) and after f) pull-out, C-PK-S-PP25-MAH75, DR=9 before g) and after h) pull-out.

DOI: https://doi.org/10.51573/Andes.PPS39.GS.FF.1

Scanning Electron Microscopy

Figure 4 shows SEM pictures of the fiber surfaces prior and after pull-out test. It can be clearly seen that adding MAH into the shell of the fibers leads to higher adhesion to the concrete. There is no significant difference in adhesion depending on the MAH-content observable.

Thermogravimetric Analysis

Figure 5 shows the results from TGA and Table 5 shows the temperature at a weight loss of 5%, 10%, 30%, and 70% mass loss. It is visible that the decomposition takes place primarily between 375°C and 525°C. Two decomposition steps are visible, which are shifted slightly by the addition of MAH. The first step is shifted to higher temperatures while the second step happens at lower temperatures.

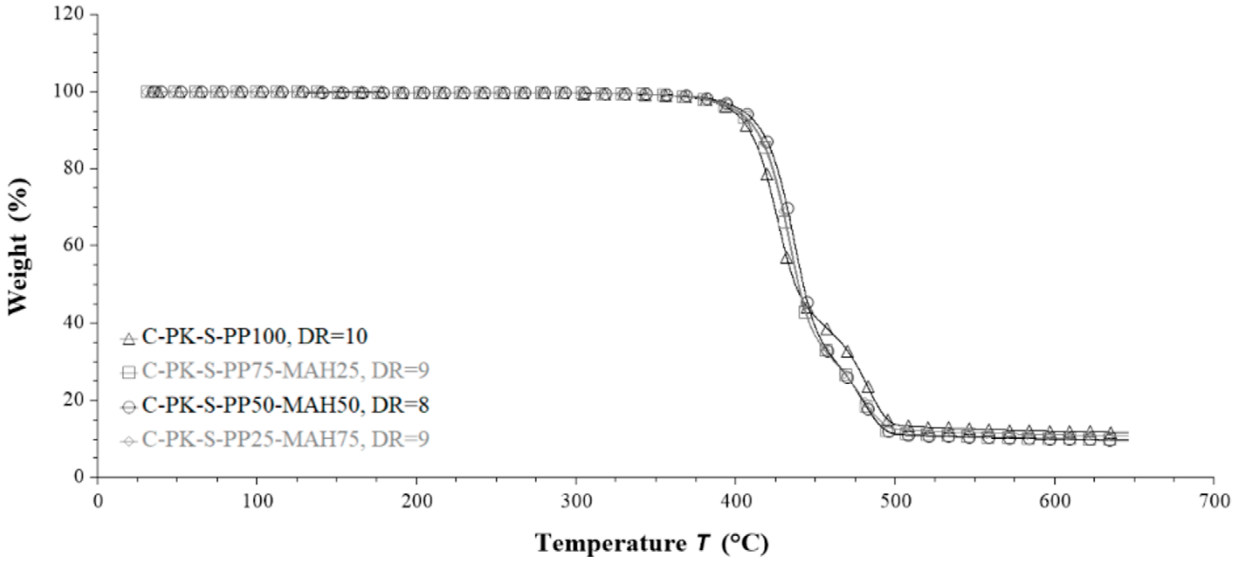

Figure 5. Results from thermogravimetric analysis.

Table 5. Temperature at certain mass loss.

Shell Material	Draw Ratio	Temperature of 5% Mass Loss	Temperature of 10% Mass Loss	Temperature of 30% Mass Loss	Temperature of 70% Mass Loss
	[1]	[°C]	[°C]	[°C]	[°C]
C-PK-S-PP100	10	398.19	408.60	424.53	474.60
C-PK-S-PP75-MAH25	9	400.29	412.61	429.06	462.77
C-PK-S-PP50-MAH50	8	404.37	415.96	432.36	462.85
C-PK-S-PP25-MAH75	9	401.53	413.28	429.75	461.81

DOI: https://doi.org/10.51573/Andes.PPS39.GS.FF.1

Conclusion

This study shows that MAH in the fiber shell has a high potential for core-shell fibers made from PK and PP. The MAH shows a positive influence on the bonding between core-shell fibers and concrete. Furthermore, MAH increases the surface energy of the fibers and concrete adheres to the fibers surface as shown by the SEM pictures. For 25 wt.-% of MAH, an increased tensile strength was observed compared to the fiber without MAH. The thermal stability is just slightly influenced by the added MAH.

The tensile strength of all fibers presented in this study surpass that of common steel rebars. The tensile strength of common steel rebars reaches values above 600 MPa. Specialized types can also reach a tensile strength of 800 MPa [13]. Accordingly, the core-shell fibers presented herein show a high potential for applications in building industries. But further research, as for instance 3-point bending tests, need to be carried out before a final conclusion can be drawn.

Acknowledgments

The authors wish to acknowledge the support of Aline Huber and Wolf Schmederer for the support of this study.

References

1. J. Hegger, M. Curbach, A. Stark, S. Wilhelm, and K. Farwig, "Innovative design concepts: Application of textile reinforced concrete to shell structures," *Structural Concrete*, vol. 19, no. 3, pp. 637–646, 2018, https://doi.org/10.1002/suco.201700157
2. U. Nürnberger and Y. Wu, "Stainless steel in concrete structures and in the fastening technique," *Materials and Corrosion*, vol. 59, no. 2, pp. 144–158, 2008, https://doi.org/10.1002/maco.200804150
3. B. Beckmann et al., "Collaborative research on carbon reinforced concrete structures in the CRC / TRR 280 project," *Civil Engineering Design*, vol. 3, no. 3, pp. 99–109, 2021, https://doi.org/10.1002/cend.202100017
4. R. Rostami, M. Zarrebini, S. B. Abdellahi, D. Mostofinejad, and S. M. Abtahi, "Investigation of flexural performance of concrete reinforced with indented and fibrillated macro polypropylene fibers based on numerical and experimental comparison," *Structural Concrete*, vol. 22, no. 1, pp. 250–263, 2021, https://doi.org/10.1002/suco.201900374
5. M. Sigrüner, D. Muscat, and N. Strübbe, "Investigation on pull-out behavior and interface critical parameters of polymer fibers embedded in concrete and their correlation with particular fiber properties," *Journal of Applied Polymer Science*, vol. 138, no. 28, p. 50745, 2021, https://doi.org/10.1002/app.50745

6. B. Wietek, *Fiber Concrete: In Construction*, 1st ed. Wiesbaden: Springer Fachmedien Wiesbaden; Imprint: Springer, 2021.

7. J. Herz, M. Sigrüner, D. Muscat, and N. Strübbe, "Co-extruded polymer fibers for concrete reinforcement," in *Proceedings of the 37th International Conference of the Polymer Processing Society (PPS-37)*, Fukuoka City, Japan, 2023, p. 80002, https://doi.org/10.1063/5.0168511

8. J. Herz, K. Lorenz, D. Muscat, and N. Strübbe, "Polymeric core-shell and mono-material fibers for concrete reinforcement," in *Proceedings of the 38th International Conference of the Polymer Processing Society (PPS-38)*, St. Gallen, Switzerland, 2024, p. 40004, https://doi.org/10.1063/5.0204946

9. RIA-Polymers GmbH, RIAMAXX HR 00 EX natur.

10. M-Base Engineering+Software GmbH, ISPLEN PP020G3E.

11. Mitsui Chemicals Europe GmbH, ADMER™ QE800E.

12. D. K. Owens and R. C. Wendt, "Estimation of the surface free energy of polymers," *Journal of Applied Polymer Science*, vol. 13, no. 8, pp. 1741–1747, 1969, https://doi.org/10.1002/app.1969.070130815

13. H. Kämpfe, Bewehrungstechnik: Grundlagen, Praxis, Beispiele, Wirtschaftlichkeit, 2nd ed. Wiesbaden, Germany: Springer Vieweg, 2020.